THE JOURNAL OF PHYSICAL CHEMISTRY B LETTERS

2006, *110,* 17706−17710
Published on Web 08/22/2006

Stabilization of Platinum Clusters by Substitutional Boron Dopants in Carbon Supports

Chethan K. Acharya and C. Heath Turner*

Department of Chemical and Biological Engineering, University of Alabama, Tuscaloosa, Alabama 35487

Received: June 9, 2006; In Final Form: August 9, 2006

To stabilize platinum clusters on carbon supports, carbon substituted boron dopants were introduced in graphite and fullerene models, and the binding energies of Pt_1 to Pt_6 clusters on the carbon supports were investigated using first-principles density functional theory (DFT) calculations. The adsorption energies of the Pt clusters increased significantly in the presence of boron. The adsorption energies of Ru_1 and Au_1 were also found to dramatically increase in the presence of boron.

Introduction

Platinum on carbon is one of the most common anode catalysts used in a PEM fuel cell. The size and stability of the nanoparticles play an important role in determining the activity of the catalyst. For instance, Yung-Eun Sung et al.[1] have observed high electrocatalytic activity of 1.7 nm PtRu, PtMo, PtW, and PtNi nanoparticles dispersed on a carbon support in a direct methanol fuel cell (DMFC). Masel et al.[2] have stated that in a direct formic acid fuel cell (DFAFC), for a highly concentrated formic acid (10, 15, and 20 M), the performance can be enhanced by increasing the surface area of the Pd nanoparticles from 23 to 60 m^2/g, and in effect reducing the size of the particles. The catalyst can lose its activity over a period of time due to the sintering of Pt nanoparticles. Sugimoto et al.[3] have claimed that particle growth is one of the causes for the loss of catalytic activity in a fuel cell. The nanoparticles have to be stabilized to minimize the propensity for sintering, which may be done by increasing the relative interaction of platinum−carbon versus platinum−platinum. In an effort to increase the interaction between the metal and the support, Group III, IV, and V substitutional dopants were introduced into graphitic carbon support models, with the intention of altering the electronic structure of the support in a beneficial way. First-principles density functional theory (DFT) calculations were used to quantify the resulting Pt-support interactions, allowing a methodical comparison of pristine and doped graphite supports. Due to the graphitic nature of the carbon model used in our calculations, the results should be comparable to an experimental sample of highly oriented pyrolitic graphite (HOPG), and these experiments are currently underway. The Group III, IV, and V elements considered here are B, N, Al, Si, and P.

Synthesis of different types of carbon with substitutional dopants such as N, B, transition metals such as Fe, Co, Ni, Rh, and Ir, and alkali metals such as Li, and K has been reported in the literature.[4−9] The property of the original carbon material changes due to the structural and electronic effects caused by the presence of the dopants in the lattice.[10−12] Several theoretical studies have previously investigated the influence of dopants in carbon on the resulting adsorption characteristics of the surface, in particular, adsorption of lithium and hydrogen. With respect to rechargeable Li ion batteries, first-principle calculations[13,14] have predicted that the presence of dopants (such as boron) will enhance Li storage and increase the reversible capacity, and this has been verified experimentally.[15] The interaction of a hydrogen atom or a hydrogen molecule with a carbon substrate has also been observed to increase in the presence of dopants such as boron, nitrogen, and alkali metals.[16−18] In other work, a nitrided carbon was experimentally and theoretically found to have a higher activity for O_2 electroreduction to H_2O_2 when compared to an untreated carbon.[19] Radovic et al.[20] have shown both experimentally and theoretically that the presence of substitutional boron suppresses O_2 chemisorption and catalyzes CO and CO_2 desorption during the carbon oxidation reaction.

In conclusion, a superficial review on the topic reveals that substitutional defects in carbon lattices have a wide gamut of influences (structural, catalytic, and electronic) on different species. In the following calculations, we find that dopants in the carbon lattice can significantly strengthen the interaction of Pt, Ru, and Au with a carbon support, suggesting a route for enhancing nanoparticle catalyst stability.

Computational Details

The present calculations are based on density functional theory (DFT) incorporated in the Gaussian03 software package,[21] using the hybrid B3LYP functional.[22] The Stuttgart/Dresden effective core potential (SDD) was used for the geometry and energy calculations of the Pt atoms and the 3-21g and 6-311g (d,p) basis sets were used to perform the carbon support geometry optimizations and energy calculations, respectively. The SDD effective core potential has been previously used to study Pt, Au, and Pd complexes[23−25] and it has been shown that the geometry parameters and frequencies were in good agreement with the experimental data. To validate the chosen model chemistry for graphite, larger basis sets such as 6-311g(d), 6-311g(d,p), 6-311+g(d,p), 6-311++g(d,p), and 6-311++g(2d,2p) were used to perform preliminary work on

* Corresponding author. E-mail: HTURNER@eng.ua.edu.

10.1021/jp063618p CCC: $33.50

the geometry optimization and energy calculation of a single Pt atom on a $C_{18}H_{10}$ graphite sheet, and all predicted similar binding energies with deviations of 0.3 kcal/mol (with a significantly higher computational cost for the larger basis sets). The graphite clusters considered here were designated as $C_{69}H_{22}X$, $C_{66}H_{21}X$, $C_{66}H_{22}B_4$, $C_{58}H_{22}B_{12}$, C_{60}, and $C_{56}B_4$, where the X represents the Group III (B and Al), IV (C and Si), and V (N and P) elements. A single layer of graphite was considered, which has been reported in the literature as a good model for the carbon support[26,27] since dispersion interactions dominate between the subsequent graphite layers. Also, it should be noted that our graphite models had greater than 13 aromatic rings (24 in $C_{67}H_{21}$ and 25 in $C_{70}H_{22}$), which is required for the formation of band structures.[28] The boron doped graphite models used in this study are shown in the Supporting Information (Figure SI 1).

A Pt atom was adsorbed on the $C_{69}H_{22}X$ and $C_{66}H_{21}X$ clusters having open and closed shell electronic configurations, depending on the X. The $C_{70}H_{22}$, $C_{66}H_{22}B_4$, and $C_{58}H_{22}B_{12}$ graphite clusters with closed shell configuration were considered for the adsorption of Pt_2 to Pt_6 clusters. To avoid the possible effects of the edges on the calculations involving the graphite sheets, fullerene models (C_{60} and $C_{56}B_4$) were also considered for the adsorption of Pt_{1-5} clusters.

The X dopant was introduced in the graphite sheet by replacing a C atom located near the center of the graphite. In the $C_{66}H_{22}B_4$ cluster, the four B atoms were also introduced in the center of the sheet. The substitutional dopants at the centers of the sheets were separated by at least two aromatic rings from the edges of the model surface, in order to minimize edge effects. In the $C_{66}H_{22}B_4$ and the $C_{56}B_4$ cluster, each boron atom was bonded to carbon atoms, without any boron−boron bonds. In the $C_{58}H_{22}B_{12}$ cluster, a carbon atom in each aromatic ring was substituted by boron, giving it a BC_5 configuration. The open and closed shell clusters with a doublet and quartet spin and singlet and triplet spin, respectively, were considered in this study.

In the calculations, the Pt atom was initially introduced on top of the dopant at a distance of 2.2 Å from the geometry-optimized graphite sheet, followed by further geometry optimization and energy calculation. The geometry-optimized Pt_2 to Pt_6 clusters were placed on top of geometry-optimized $C_{70}H_{22}$, $C_{66}H_{22}B_4$, and $C_{58}H_{22}B_{12}$ cluster models at an initial separation of 2.2 Å. The same general procedure was adopted for the calculations involving the fullerene support. The geometry of the Pt_{1-6}/graphite system was fully optimized, with respect to the coordinates of all of the atoms, with the exception of the edge atoms of the graphite sheet, which were constrained. No constraints were imposed on the fullerene clusters. Corrections for basis set superposition error (BSSE) were found to be insignificant when estimated during preliminary calculations, and were therefore neglected. It should be emphasized that, in addition to the structures of the Pt clusters considered here, there could be other isomers of Pt that are also stable on the carbon models. However, only the minimum energy structures were considered here. Finally, as a further extension of our work, the binding energies of other metals on fullerene supports were investigated. Using the same SDD effective core potential, we report the binding energies of a single Au and Ru atom on pristine and boron-doped fullerenes.

Results and Discussion

The first requirement of the doped carbon substrates is that the structural integrity of the support should be maintained. To analyze the instability introduced by the dopants, the heat of formation (ΔH_f) of the $C_{69}H_{22}X$ and the $C_{66}H_{21}X$ clusters were calculated when X was substituted at the center and at the edge as shown in Table 1. These values were compared against the pristine graphite sheets by calculating the difference in the ΔH_f between them (the difference denoted as ΔE), where ΔH_f was calculated using the expression

TABLE 1: Characterization of the $C_{69}H_{22}X$ and $C_{66}H_{21}X$ Clusters with X Located at the Center and at the Edge

cluster	ES	ΔH_f (kcal/mol)	ΔE (kcal/mol)
substitution at the center of the graphite sheet			
$C_{69}H_{22}B$	open	−15811.61	94.44
$C_{70}H_{22}$	close	−15906.05	0.00
$C_{69}H_{22}N$	open	−15783.24	122.81
$C_{69}H_{22}Al$	open	−15607.54	298.51
$C_{69}H_{22}Si$	close	−15688.37	217.68
$C_{69}H_{22}P$	open	−15672.87	233.18
$C_{66}H_{21}B$	close	−15141.74	96.51
$C_{67}H_{21}$	open	−15238.25	0.00
$C_{66}H_{21}N$	close	−15113.19	125.06
$C_{66}H_{21}Al$	close	−14938.87	299.38
$C_{66}H_{21}Si$	open	−15020.51	217.74
$C_{66}H_{21}P$	close	−15001.93	236.32
substitution at the edge of the graphite sheet			
$C_{69}H_{22}B$	open	−15818.82	87.23
$C_{70}H_{22}$	close	−15906.05	0.00
$C_{69}H_{22}N$	open	−15791.03	115.02
$C_{69}H_{22}Al$	open	−15695.90	210.15
$C_{69}H_{22}Si$	close	−15746.16	159.89
$C_{69}H_{22}P$	open	−15724.82	181.23
$C_{66}H_{21}B$	close	−15148.46	89.79
$C_{67}H_{21}$	open	−15238.25	0.00
$C_{66}H_{21}N$	close	−15120.78	117.47
$C_{66}H_{21}Al$	close	−15021.45	216.80
$C_{66}H_{21}Si$	open	−15078.17	160.08
$C_{66}H_{21}P$	close	−15054.71	183.54

$$\Delta H_f = E_{cluster} - n^*E_C - m^*E_H - E_X \quad (1)$$

In this expression, $E_{cluster}$, E_C, E_H, and E_X are the electronic energies of cluster, carbon, hydrogen, and dopant atom in kcal/mol and n and m are the number of carbon and hydrogen atoms in the graphite cluster, respectively. The table also shows the electronic state (ES) of each cluster, either open or closed shell.

All of the graphite sheets retained their planarity even after performing geometry relaxations. Among the dopants considered, the boron atom created the least instability, while the ΔE value increased as we moved down the periodic table. The substitution of a carbon by a dopant at the center of the graphite sheet created greater instability than the corresponding edge substitution because the neighboring carbon atoms of the dopant at the center have a higher coordination number than the edge dopant neighbors, creating a greater disturbance in the graphite lattice.

A Pt atom placed on top of the dopant preferred to adsorb on the 2-fold bridge site and was more stable than the on-top or the hollow site. The adsorption energy or the binding energy (BE) per Pt atom on a graphite sheet was calculated by the expression

$$\mathrm{BE/Pt} = \frac{(E_{(\mathrm{graphite}+\mathrm{Pt}_n)} - E_{\mathrm{graphite}} - E_{\mathrm{Pt}_n})}{n} \quad (2)$$

where $E_{(\mathrm{graphite}+\mathrm{Pt}_n)}$ is the total energy of the cluster containing Pt_n adsorbed on graphite and E_{graphite} and E_{Pt_n} are the energies of the separated groups, all expressed in kcal/mol. A negative value of binding energy corresponds to a stable adsorption of a

TABLE 2: Binding Energy of a Pt_1 Atom on Pristine, Boron, and Nitrogen-doped Graphite with Closed and Open Shell Configurations[a]

cluster	ES	BE/Pt (kcal/mol)	ΔD (Å)
	pristine graphite sheet		
$C_{70}H_{22}$	close	−12.49	0.29
$C_{67}H_{21}$	open	−9.41	0.29
	boron-doped graphite sheet		
$C_{66}H_{21}B$	close	−18.57	0.21
$C_{69}H_{22}B$	open	−18.76	0.25
	nitrogen-doped graphite sheet		
$C_{66}H_{21}N$	close	−5.58	0.38
$C_{69}H_{22}N$	open	−9.04	0.22
	pristine graphite sheet with the Pt atom at the edge		
$C_{70}H_{22}$	close	−32.82	
$C_{67}H_{21}$	open	−32.19	
	edge boron-doped graphite sheet with the Pt atom at the edge		
$C_{66}H_{21}B$	close	−53.28	
$C_{69}H_{22}B$	open	−55.53	

[a] ΔD represents the maximum displacement of the atoms in graphite from planarity. Binding energy of a Pt atom on pristine and boron-doped graphite substrates, with the carbon at the edge substituted by boron is also given in the table.

Pt_n cluster on graphite, with stronger adsorption indicated by more negative values.

When the adsorption of the Pt_1 atom was optimized on the graphite substrates, the Al, Si, and P atoms near the center protruded out of the graphite plane, causing moderate distortions from the usual planar surface of pristine graphite. It could be due to the size of the dopants, which caused instability in the graphite lattice, evident from the ΔE values in Table 1. For this reason, these three elements were not considered in further calculations. However, this decision should not be interpreted to indicate that these elements should necessarily be excluded from other investigations in the future. The pictures of the Pt_1 atom adsorbed on the $C_{66}H_{21}X$ graphite sheets are shown in the Supporting Information (Figure SI 2).

Table 2 shows the binding energies of the Pt_1 atom with the $C_{70}H_{22}$, $C_{66}H_{21}B$, and $C_{66}H_{21}N$ graphite substrates having a closed shell configuration, as well as with the $C_{67}H_{21}$, $C_{69}H_{22}B$, and $C_{69}H_{22}N$ graphite substrates having an open shell configuration. The adsorption energies of the Pt atom adsorbed on the edge will be discussed later. It can be seen from the table that the binding energy of the Pt atom in the presence of boron is increased, while it is decreased in the presence of nitrogen, relative to the pristine graphite sheet. The table also gives the maximum displacement of the atoms in graphite from planarity after the adsorption of the Pt atom. The maximum displacement was observed in the nitrogen-doped graphite (0.38 Å) followed by pristine (0.29 Å) and boron-doped graphite (0.25 Å).

The difference in the binding energy of the Pt atom on the pristine, boron-doped, and nitrogen-doped graphite sheets can be explained in terms of frontier orbital theory. The highest occupied molecular orbital (HOMO) and the lowest unoccupied molecular orbital (LUMO) of the different graphite models with a closed shell electronic configuration are given in Table 3. The LUMO of the boron-doped graphite is increased (more negative) when compared to the pristine graphite. There is one less electron in the cluster due to the introduction of boron, which results in a decrease in the gap between the HOMO of the Pt_1 atom and the LUMO of the boron-doped graphite. As a result, the electrons can easily transfer from the Pt atom to the graphite cluster, leading to an increase in the adsorption energy. When a comparison of the HOMO and LUMO of the nitrogen-doped graphite with the pristine graphite model is made, the HOMO of the nitrogen-doped graphite decreased significantly (less negative) without affecting the LUMO energy, which indicates that the nitrogen-doped graphite prefers to donate electrons to the Pt atom, limiting the electron transfer and the binding energy of the Pt atom. The difference between the HOMO of the nitrogen-doped graphite and the LUMO of the Pt atom is positive, as opposed to a negative gap between the pristine graphite and the Pt atom. Kurita et al.[14] attributed the increase in the adsorption energy of Li atoms on boron-substituted carbons to the shift in the LUMO energies. Based on the results obtained for the adsorption energies of a Pt atom on the different graphite models, the pristine and boron-doped graphite models were considered for further studies. It should be emphasized that the nitrogen-doped graphite models cannot be discarded from future studies because the system considered here was not comprehensive. It was not pursued here, mainly to focus our calculations on the most interesting system. The HOMO and LUMO energies of the other boron-doped graphite models used for the adsorption of Pt_2 to Pt_6 clusters is also given in Table 3, and the pictures of the Pt_1 atom adsorbed on these three graphite models are shown in the Supporting Information (Figure SI 2a−c).

TABLE 3: HOMO and LUMO Energies of the Graphite Models with a Closed Shell Electronic Configuration, and Their Energy Gap with the Pt_1 Atom[a]

graphite models	HOMO	LUMO	HOMO(Pt_1)−LUMO(graphite)	HOMO(graphite)−LUMO(Pt_1)
$C_{70}H_{22}$	−102.68	−74.97	−76.83	−2.55
$C_{66}H_{21}B$	−102.47	−89.38	−62.41	
$C_{66}H_{21}N$	−88.59	−74.49		11.54
$C_{66}H_{22}B_4$	−102.69	−85.94		
$C_{58}H_{22}B_{12}$	−128.06	−113.62		

[a] All the energies are in kcal/mol.

Before considering the results of the larger Pt_n clusters, we examined the adsorption energies of the Pt_1 atom at the edge of pristine and boron-doped (doped at the edge) graphite models, and the results are shown in Table 2. Even at the edge, the Pt_1 atom prefers to adsorb on the 2-fold bridge site. The binding energy of the Pt atom in the presence of the boron dopant was greater than the pristine graphite by more than 20 kcal/mol. The binding energy of the Pt atom at the edge of the cluster was greater than at the centers, which was due to the higher electron density on the edge carbon atoms.

The $C_{66}H_{22}B_4$ (5 wt % of B) and $C_{58}H_{22}B_{12}$ (15.3 wt % of B) clusters, which retained planarity even after geometry optimization, were considered for the adsorption of the Pt_2 to Pt_6 clusters. The binding energy per Pt atom on the boron-doped graphite clusters was calculated and compared with the pristine graphite sheet, as shown in Table 4. The table also shows the maximum displacement of the atoms in graphite from planarity during the adsorption of the Pt clusters. The adsorption energy of the Pt clusters and the maximum displacement of the atoms in graphite were greatest on $C_{66}H_{22}B_4$ (−36 kcal/mol and 0.83 Å) followed by $C_{58}H_{22}B_{12}$ (−19 kcal/mol and 0.42 Å) and the $C_{70}H_{22}$ cluster (−4.5 kcal/mol and 0.30 Å). Wang et al.[27] reported the adsorption energy of the Pt_{37} cluster adsorbed on the pristine graphite support to be −1.68 kcal, per Pt atom, which is close to the results obtained here. The binding energies of the Pt clusters were greater in $C_{66}H_{22}B_4$ because the LUMO energy, given in Table 3, increased without affecting the HOMO energy when compared to the pristine graphite. Moreover, it was a local defect, which was not the case in the $C_{58}H_{22}B_{12}$ graphite. In the $C_{58}H_{22}B_{12}$ cluster, the LUMO energy was more

TABLE 4: Binding Energy per Pt Atom in Pt_{2-6} Clusters Adsorbed on Pristine ($C_{70}H_{22}$), 5 wt % B Doped ($C_{66}H_{22}B_4$), and 15.3 wt % B Doped ($C_{58}H_{22}B_{12}$ in BC_5 Configuration) Graphite Sheet

cluster	ES	BE/Pt (kcal/mol)	ΔD (Å)
	$Pt_{2-6}/C_{70}H_{22}$ system		
$Pt_2 + C_{70}H_{22}$	close	−3.67	0.30
$Pt_3 + C_{70}H_{22}$	close	−4.50	0.14
$Pt_4 + C_{70}H_{22}$	close	−1.77	0.15
$Pt_5 + C_{70}H_{22}$	close	−4.33	0.16
$Pt_6 + C_{70}H_{22}$	close	−4.47	0.09
	$Pt_{2-6}/C_{66}H_{22}B_4$ system		
$Pt_2 + C_{66}H_{22}B_4$	close	−35.99	0.59
$Pt_3 + C_{66}H_{22}B_4$	close	−16.52	0.44
$Pt_4 + C_{66}H_{22}B_4$	close	−20.06	0.69
$Pt_5 + C_{66}H_{22}B_4$	close	−18.80	0.53
$Pt_6 + C_{66}H_{22}B_4$	close	−17.36	0.83
	$Pt_{2-6}/C_{58}H_{22}B_{12}$ system		
$Pt_2 + C_{58}H_{22}B_{12}$	close	−18.95	0.19
$Pt_3 + C_{58}H_{22}B_{12}$	close	−15.19	0.15
$Pt_4 + C_{58}H_{22}B_{12}$	close	−12.13	0.15
$Pt_5 + C_{58}H_{22}B_{12}$	close	−14.38	0.38
$Pt_6 + C_{58}H_{22}B_{12}$	close	−12.47	0.42

than the $C_{66}H_{22}B_4$ cluster, but at the same time, the HOMO energy increased, which counter-balanced the increase in the LUMO energy, and thus limited the adsorption energy of the Pt atoms. The calculated values in Table 4 tend to indicate that the increased adsorption energies (due to boron doping) would be seen even with larger Pt_n clusters, since the enhanced binding energy does not decrease with respect to cluster size. The Pt_6 cluster adsorbed on various graphite models is shown in the Supporting Information (Figure SI 3).

To see if the same phenomenon in the binding energy exists for other forms of carbon, a C_{60} fullerene was considered as a carbon support. Also, the fullerene models are not complicated by the issue of edge termination, allowing for a more rigorous model of the structure. The Pt_{1-5} clusters were adsorbed on a pristine and on a $C_{56}B_4$ fullerene. The Pt_1 atom preferred to adsorb on the 2-fold bridge site common to two adjacent six member aromatic rings in the pristine and the boron-doped fullerene. It was more stable than the bridge site common to adjacent five and six member aromatic rings, or the on-top or hollow sites. The binding energies of the Pt_{1-5} clusters on the two types of fullerenes are shown in Table 5. The drop in the binding energy per Pt atom in Pt_1 to Pt_3 clusters could be due to the curvature of the support, which reduces the contact between the Pt atoms and the support. This artifact becomes less prominent in larger clusters, as expected. The LUMO energies of pristine and boron-doped fullerene models were −83.89 and −107.21 kcal/mol, respectively, and the HOMO energies were −148.18 and −133.01 kcal/mol. The LUMO energy of the boron-doped fullerene increased significantly, with a decrease in the HOMO energy, both favoring the adsorption of the Pt atom. The shifts in the LUMO energies affected the gap between the HOMO of the Pt atom and the LUMO of the fullerene models, as shown in Table 5. The adsorption energy per Pt in the Pt_{1-5} clusters was greater on the boron-doped fullerene than on the pristine fullerene by as much as ∼16 kcal/mol. This is consistent with our results obtained on the graphitic supports. The HOMO and the LUMO iso surfaces of the adsorption of the Pt_1 atom on the pristine and the boron-doped fullerenes are shown in Figure 1. The interface between Pt_1 and the boron-doped fullerene had a greater electron density accumulation than the Pt atom and the pristine fullerene, which agrees with the higher binding energy results obtained for the Pt atom adsorbed on the boron-doped fullerenes.

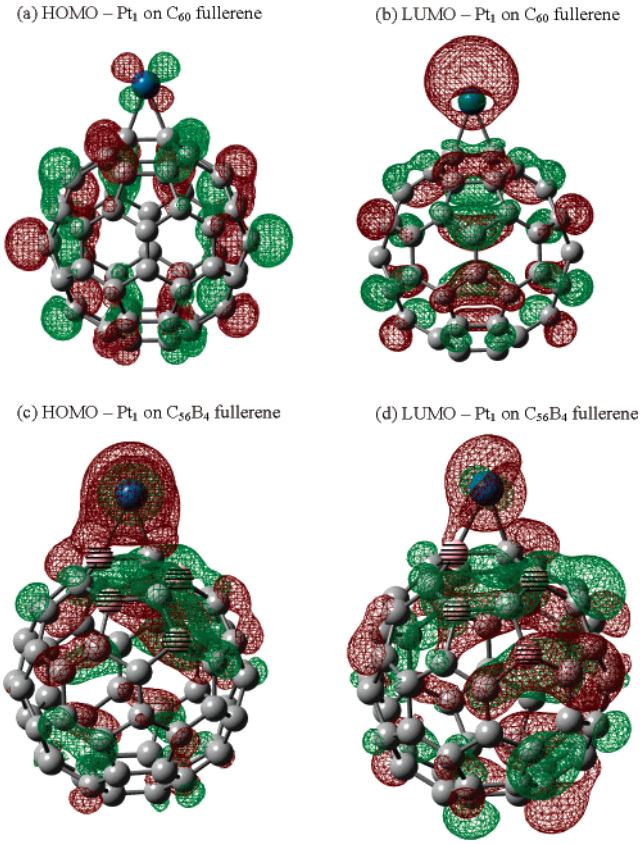

Figure 1. Surfaces of HOMO and LUMO for the adsorption of Pt_1 on fullerenes. The range of iso surface values is ±0.02 e/Å^3. The green color represents electron accumulation and the brown color represents electron depletion. The atoms with horizontal stripes in boron-doped fullerene ($C_{56}B_4$) represent boron.

To see if the boron doping increased the adsorption energy of other catalytic metals, a gold and a ruthenium atom was adsorbed on the C_{60} and $C_{56}B_4$ fullerene support, and the adsorption energies are given in Table 5. The presence of boron in the fullerene increased the adsorption energy of the Au and Ru atoms significantly (∼40 kcal/mol for Au and ∼42 kcal/mol for Ru). The Au atom preferred the carbon on-top site, both

TABLE 5: Binding Energy per Pt Atom in Pt_{1-5} Clusters, the Au_1, and the Ru_1 Atom on Pristine and Boron-Doped Fullerene[a]

cluster	BE/M	cluster	BE/M	HOMO(M_1)−LUMO(C_{60})	HOMO(M_1)−LUMO($C_{56}B_4$)
$Pt_1 + C_{60}$	−54.09	$Pt_1 + C_{56}B_4$	−67.46	−67.91	−44.58
$Pt_2 + C_{60}$	−27.99	$Pt_2 + C_{56}B_4$	−44.30		
$Pt_3 + C_{60}$	−11.86	$Pt_3 + C_{56}B_4$	−25.50		
$Pt_4 + C_{60}$	−8.89	$Pt_4 + C_{56}B_4$	−24.32		
$Pt_5 + C_{60}$	−8.22	$Pt_5 + C_{56}B_4$	−21.56		
$Au_1 + C_{60}$	−6.28	$Au_1 + C_{56}B_4$	−46.81	−69.11	−45.78
$Ru_1 + C_{60}$	−59.43	$Ru_1 + C_{56}B_4$	−101.84	−23.39	−0.07

[a] The HOMO and LUMO gap between the M = (Pt, Au, and Ru)$_1$ and the C_{60} and $C_{56}B_4$ fullerene. All the energies are in kcal/mol.

in the presence and absence of boron. In the presence of boron the Au atom adsorbed on top of the carbon atom bonded to boron (not actually to boron itself). The Ru atom, like the Pt atom, preferred to adsorb on the bridge site common to two adjacent six-member aromatic rings, both on the pristine and on the boron-doped fullerene. The Ru atom had higher adsorption energy than Pt on the pristine fullerene, which is consistent with the results of Wang et al.[27] who have also studied Ru−C and Pt−C interactions. In addition, the high adsorption energy of the Ru atom on the boron-doped fullerene caused the rupture of the spherical fullerene structure and the Ru atom became incorporated into the carbon lattice. The energy gap between the HOMO of the Au atom and the LUMO of the boron-doped fullerene, as shown in Table 5, was slightly greater than the gap for the $Pt/C_{56}B_4$ system, which might be the reason for the lowering of the binding energy of the Au atom. The energy gap between the HOMO of the Ru atom and the LUMO of the $C_{56}B_4$ fullerene was very small, which might be the reason for the high adsorption energy. The Pt_5, Au_1, and Ru_1 atoms adsorbed on C_{60} and $C_{56}B_4$ supports are shown in the Supporting Information (Figure SI 4). The fullerene rupture upon Ru adsorption may have beneficial or detrimental effects, depending upon the application. If the fullerene is intended to deliver an active species to a specific target, a B-doped fullerene opening event could be triggered by an encounter with Ru.

Conclusions

The results presented in this work clearly show that the presence of substitutional boron defects in carbon supports increases the adsorption energy of the metal atoms Pt, Au, and Ru. The adsorption energy was increased by a greater magnitude in cases where the carbon supports were doped along their edges. The adsorption enhancements that we predict may potentially be used to stabilize catalyst nanoparticles on carbon supports, and experiments are currently underway to test this possibility. Also, one may imagine the opposite case to what we have explored here, where the adsorbent is a fullerene and the substrate is a metal surface. It is expected that doping a fullerene with boron will increase the affinity of the fullerene for the surface, depending on the metal or alloy used as the substrate.

Acknowledgment. Funding for this work was provided by DOE EPSCoR, grant #DE-FG02-01ER45867. Supercomputer resources were provided by the Alabama Supercomputer Center and the Pacific Northwest National Lab EMSL facility.

Supporting Information Available: Pictures of: (a) Boron-doped graphite models used for Pt cluster adsorption; (b) geometry optimized structures of Pt_1 atom on different closed shell graphite models; (c) geometry optimized Pt_6 cluster on different graphite models; and (d) geometry optimized Pt_5, Au_1, and Ru_1 clusters on pristine and boron-doped fullerene models. This material is available free of charge via the Internet at http://pubs.acs.org.

References and Notes

(1) Lee, S.-A.; Park, K.-W.; Choi, J.-H.; Kwon, B.-K.; Sung, Y.-E. *J. Electrochem. Soc.* **2002**, *149*, 1299.
(2) Zhu, Y.; Khan, Z.; Masel, R. I. *Proc. Electrochem. Soc.* **2004**, *206*, 1517.
(3) Kawaguchi, T.; Sugimoto, W.; Murakami, Y.; Takasu, Y. *J. Catal.* **2005**, *229*, 176.
(4) Shirasaki, T.; Derre, A.; Menetrier, M.; Tressaud, A.; Flandrois, S. *Carbon* **2000**, *38*, 1461.
(5) Morinobu, E.; Takuya, H.; Seong-Hwa, H.; Toshiaki, E.; Milred, S. D. *J. Appl. Phys.* **2001**, *90*, 5670.
(6) Czerw, R.; Terrones, M.; Charlier, J. C.; Blase, X.; Foley, B.; Kamalakaran, R.; Grobert, N.; Terrones, H.; Tekleab, D.; Ajayan, P. M.; Blau, W.; Ruhle, M.; Carroll, D. L. *Nano Lett.* **2001**, *1*, 457.
(7) Naeini, J. G.; Way, B. M.; Dahn, J. R.; Irwin, J. C. *Phys. Rev. B* **1996**, *54*, 144.
(8) Branz, W.; Billas, I. M. L.; Malinowski, N.; Tast, F.; Heinebrodt, M.; Martin, T. P. *J. Chem. Phys.* **1998**, *109*, 3425.
(9) Chen, P.; Wu, X.; Lin, J.; Tan, K. L. *Science* **1999**, *285*, 91.
(10) Veronica, B.; Juan, E. P.; Jamal, U.; Gustavo, E. S. *J. Chem. Phys.* **2006**, *124*, 024709.
(11) Sylvain, L.; Stephan, R.; Didier, M.; Jean-Christophe, C. *Phys. Rev. Lett.* **2004**, *92*, 256805.
(12) Nevidomskyy, A. H.; Csanyi, G.; Payne, M. C. *Phys. Rev. Lett.* **2003**, *91*, 105502.
(13) Song, M. K.; No, K. T. *J. Electrochem. Soc.* **2004**, *151*, 1696.
(14) Kurita, N. *Carbon* **2000**, *38*, 65.
(15) Yin, G.; Gao, Y.; Shi, P.; Cheng, X.; Aramata, A. *Mater. Chem. Phys.* **2003**, *80*, 94.
(16) Froudakis, G. E. *Nano Lett.* **2001**, *1*, 531.
(17) Zhu, Z. H.; Hatori, H.; Wang, S. B.; Lu, G. Q. *J. Phys. Chem. B* **2005**, *109*, 16744.
(18) Zhu, Z. H.; Lu, G. Q.; Hatori, H. *J. Phys. Chem. B* **2006**, *110*, 1249.
(19) Sidik, R. A.; Anderson, A. B.; Subramanian, N. P.; Kumaraguru, S. P.; Popov, B. N. *J. Phys. Chem. B* **2006**, *110*, 1787.
(20) Radovic, L. R.; Karra, M.; Skokova, K.; Thrower, P. A. *Carbon* **1998**, *36*, 1841.
(21) Frisch, M. J.; Trucks, G. W.; Schlegel, H. B.; Scuseria, G. E.; Robb, M. A.; Cheeseman, J. R.; Montgomery, J. A., Jr.; Vreven, T.; Kudin, K. N.; Burant, J. C.; Millam, J. M.; Iyengar, S. S.; Tomasi, J.; Barone, V.; Mennucci, B.; Cossi, M.; Scalmani, G.; Rega, N.; Petersson, G. A.; Nakatsuji, H.; Hada, M.; Ehara, M.; Toyota, K.; Fukuda, R.; Hasegawa, J.; Ishida, M.; Nakajima, T.; Honda, Y.; Kitao, O.; Nakai, H.; Klene, M.; Li, X.; Knox, J. E.; Hratchian, H. P.; Cross, J. B.; Bakken, V.; Adamo, C.; Jaramillo, J.; Gomperts, R.; Stratmann, R. E.; Yazyev, O.; Austin, A. J.; Cammi, R.; Pomelli, C.; Ochterski, J. W.; Ayala, P. Y.; Morokuma, K.; Voth, G. A.; Salvador, P.; Dannenberg, J. J.; Zakrzewski, V. G.; Dapprich, S.; Daniels, A. D.; Strain, M. C.; Farkas, O.; Malick, D. K.; Rabuck, A. D.; Raghavachari, K.; Foresman, J. B.; Ortiz, J. V.; Cui, Q.; Baboul, A. G.; Clifford, S.; Cioslowski, J.; Stefanov, B. B.; Liu, G.; Liashenko, A.; Piskorz, P.; Komaromi, I.; Martin, R. L.; Fox, D. J.; Keith, T.; Al-Laham, M. A.; Peng, C. Y.; Nanayakkara, A.; Challacombe, M.; Gill, P. M. W.; Johnson, B.; Chen, W.; Wong, M. W.; Gonzalez, C.; Pople, J. A. *Gaussian 03*, revision C.02; Gaussian, Inc.: Wallingford, CT, 2004.
(22) Axel, D. B. *J. Chem. Phys.* **1993**, *98*, 5648.
(23) Stringer, K. L.; Citir, M.; Metz, R. B. *J. Phys. Chem. A* **2004**, *108*, 6996.
(24) Yang, G.; Jin, C.; Hong, J.; Guo, Z.; Zhu, L. *Spectrochim. Acta A* **2004**, *60*, 3187.
(25) Zhang, Y.; Zhang, L.; Tao, H.; Sun, X.; Zhu, L. *Spectrochim. Acta A* **2003**, *59*, 493.
(26) Moullet, I. *Surf. Sci.* **1995**, *331−333*, 697.
(27) Wang, L. L.; Khare, S. V.; Chirita, V.; Johnson, D. D.; Rockett, A. A.; Frenkel, A. I.; Mack, N. H.; Nuzzo, R. G. *J. Am. Chem. Soc.* **2006**, *128*, 131.
(28) Coulson, C. A. F.; Schaad, L. J.; Burnelle, L. In *Proceedings of the Third Conference on Carbon* **1959**, 27.